Zeitschrift für Kristallographie 175, 15–30 (1986)

Enumeration of 4-connected 3-dimensional nets and classification of framework silicates. 3*D* nets based on insertion of 2-connected vertices into 3-connected plane nets

Frank C. Hawthorne* and Joseph V. Smith

Department of the Geophysical Sciences, The University of Chicago, Chicago, Illinois 60637 USA

Received: April 11, 1985; in revised form May 30, 1985

Nets / Frameworks / Beryl / Milarite / Steacyite

Abstract. Insertion of a 2-connected vertex into alternate edges of a 2*D* net leads to a new family of 3*D* nets. The simplest operation is conversion of 2-connected vertices of adjacent parallel 2*D* nets into a square-planar vertex. Relative rotation of tetrahedral vertices above and below each square-planar vertex converts it into a tetrahedral vertex. The simpler nets of each type are enumerated for the 6^3, 3.12^2, 4.8^2 and 4.6.12 2*D* nets; these nets have higher symmetry and less geometrical distortion than the infinity of nets which are not listed. A further set of nets is obtained by applying a sigma transformation in the plane of each original 2*D* net. The structures of the beryl and milarite groups of minerals are based on 3*D* nets obtained from the 6^3 net, and that of steacyite from the 4.8^2 net.

Introduction

Parts I–VIII of this series (Smith, 1977, 1978, 1979, 1983; Smith and Bennett, 1981, 1984; Smith and Dytrych, 1984; Bennett and Smith, 1985) have progressively enumerated 4-connected 3-dimensional nets, primarily by considering different possible linkages between congruent 3-connected 2-dimensional nets. In this ninth paper, we introduce a new operation, the insertion of a 2-connected vertex into some edges of a 3-connected 2-

* *Permanent address:* Department of Earth Sciences, University of Manitoba, Winnipeg, Manitoba, Canada R3T 2N2

dimensional net. Each 2-connected vertex is converted into a 4-connected one by merging it with a 2-connected vertex from an adjacent modified $2D$ net. Two families of $3D$ nets are produced by arranging the four edges incident at each new 4-connected vertex in either a tetrahedral or square-planar geometry. The first family is of particular relevance to nets of silicates and other tetrahedrally-coordinated materials, and the second family provides a theoretical basis for possible frameworks incorporating both tetrahedral and square-planar chemical units. Furthermore, addition of two branches to each square-planar unit produces an octahedron. Members of the first family of nets are represented by at least 16 minerals containing various elements including Li, Be, Mg, Fe^{2+} and Fe^{3+}, as well as Si, Al and P which are particularly important in molecular-sieve technology.

Enumeration: General relations

We consider only the regular and semi-regular 3-connected plane nets 6^3, 3.12^2, 4.8^2 and 4.6.12. An edge will be identified by its adjacent polygons; thus 4.8 is common to a square and an octagon in the 4.8^2 net, and 6^2 is an edge in the 6^3 net.

A piece of a plane net is represented (Fig. 1a) by six 3-connected vertices connected by edges of equal length. A 2-connected vertex r (filled circle) is inserted into an edge pq. The simplest way to generate a 4-connected $3D$ net is to place congruent nets (dashed lines; vertices p',q') directly above and below the initial net. The vertices $pqp'q'r$ are then adjusted so that r lies at the center of the square $pqp'q'$ (Fig. 1b). Each vertex (e.g. p) retains two edges from the initial 3-connected $2D$ net (e.g. ps, pt). The "half-edge" pr is elongated into an edge of equal length to ps and pt, and a new edge $p'r$ is added. The new vertices r and r' are also 4-connected. In plan (Fig. 1a, right), the square $pqq'p'r$ appears as two line segments with $pr = rq = (ps = pt)/\sqrt{2}$. From the topological viewpoint, of course, equality of the edges is not necessary, and only the connectivity is important. From the chemical viewpoint, equality of the edges is also not necessary; in particular, vertices p, q and r would be expected to be occupied by different chemical species because of the difference in angular orientation.

In order to obtain a similar angular environment for all the vertices, each piece of a $2D$ net is rotated about r in an opposite direction to the two adjacent nets (Fig. 1c, d). The vertices $pqp'q'$ adopt a tetrahedral arrangement about r, which would become regular for a particular value of prq'. For an actual material of composition TO_2, where T is a species tetrahedrally-coordinated to oxygen, the regularity of the tetrahedra around T_1 vertices at p, p', q and q', and around T_2 vertices at r, r' is

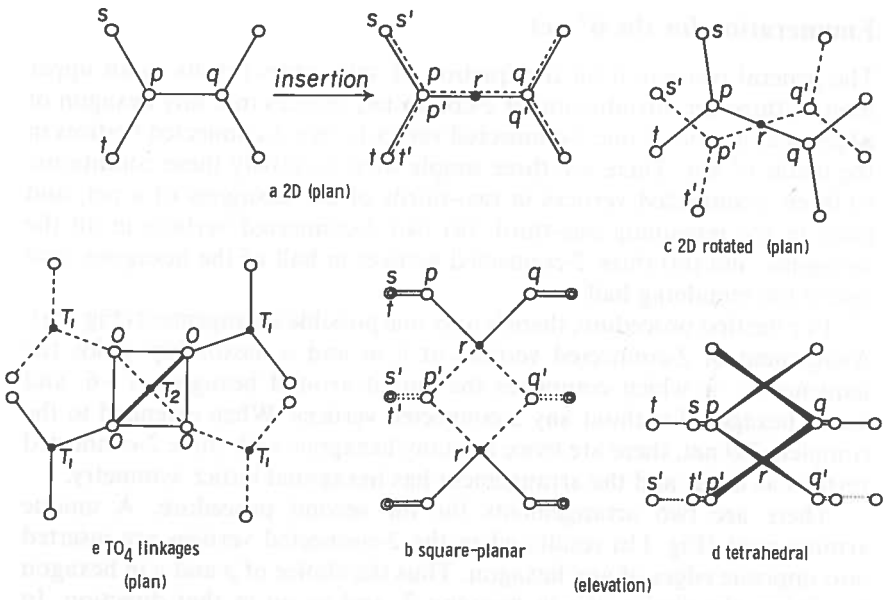

Fig. 1. The insertion operation and the geometrical relationships for square-planar and tetrahedral linkages. (a) Plan of the insertion of vertex r into edge pq of a piece of a $2D$ net, and conversion of r into a square-planar linkage between vertices p and q of an upper net (continuous line) and p' and q' of a lower net (dashed line). (b) Elevation of the square-planar linkage. (c) Plan of the relative rotation of adjacent parts of $2D$ nets required to give a tetrahedral arrangement of p, q, p' and q' about r. (d) Elevation of the tetrahedral linkage, with tapering of lines to show the perspective. (e) Plan of a piece of a TO_4 framework showing the tetrahedral linkage around the T_2 site at r

determined by the T – O – T angles (Fig. 1 e). In this paper, we shall consider first the connectivity of each new $3D$ net, and then the geometrical consequences for any chemical material based on each net. Particularly important is whether local rotation of pieces of adjacent $2D$ nets enforces a different connectivity on vertices in the resulting $3D$ net.

Each net produced by the above procedures can be changed into another net by applying a σ-transformation (Shoemaker, Robson and Broussard, 1973) in the plane of each prototype $2D$ net. Addition of a mirror plane converts each 4-connected vertex of type p, q, s and t into a pair of 4-connected vertices connected by a vertical edge. Because application of a σ-transformation to vertex r would produce two 3-connected vertices joined by a vertical edge, it is not considered here.

Finally, there is a simple restriction on the fraction of split edges in a 3-connected $2D$ net. Each 3-connected vertex must retain two out of the three edges, as the remaining third edge is converted into two edges to give a 4-connected net.

Enumeration for the 6^3 net

The general restriction on the fraction of split edges results in an upper limit of three for introduction of 2-connected vertices into any hexagon of edges, and a ratio of one 2-connected vertex to two 3-connected vertices in the whole 6^3 net. There are three simple ways to satisfy these conditions: (i) three 2-connected vertices in two-thirds of the hexagons of a net, and none in the remaining one-third, (ii) two 2-connected vertices in all the hexagons, and (iii) three 2-connected vertices in half of the hexagons, and one in the remaining half.

For the first procedure, there is only one possible arrangement (Fig. 2a). Assignment of 2-connected vertices at *l*, *m* and *n* inexorably yields the sequence $o-w$ which completes the circuit around hexagons $1-6$, and leaves hexagon 7 without any 2-connected vertices. When extended to the complete $2D$ net, there are twice as many hexagons with three 2-connected vertices as none, and the arrangement has hexagonal lattice symmetry.

There are two arrangements for the second procedure. A unique arrangement (Fig. 1b) results when the 2-connected vertices are inserted into opposite edges of any hexagon. Thus the choice of *p* and *q* in hexagon 1 enforces the choice of *r* in hexagon 2, and so on in that direction. In hexagon 3, *s* and *t* must be chosen, and so on for *u*, *v*, and *w* in hexagons 4 and 5. Another unique arrangement (Fig. 1c) results when the two 2-connected vertices are separated by an unmodified edge. Assignment of *p*

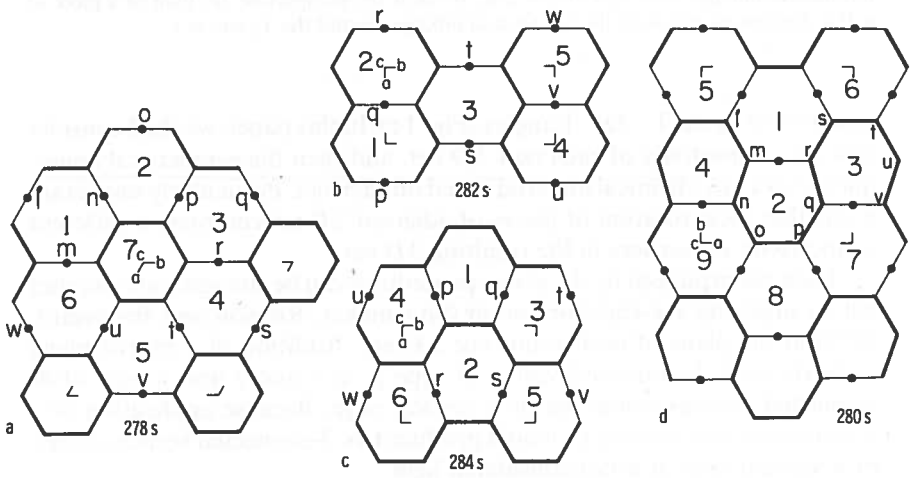

Fig. 2. Plans of the simple nets obtained by insertion of square-planar 4-connected vertices between parallel 6^3 nets. Each plan represents two nets: the one listed by the number (n) and a second net ($n + 1$) obtained by a $\sigma(h)$ transformation in the plane of each 6^3 net. Each unmodified edge is shown in heavy line, and each modified edge is increased in length by $\sqrt{2}$ and shown by a narrow line segment straddling the square-planar vertex

and q in hexagon 1 enforces the choice of r and s in hexagon 2, t in 3, u in 4, v in 5, w in 6 and so on.

The third procedure also gives a unique arrangement, and the concept of infinite path provides the simplest demonstration. Returning to Figs. 2b and 2c, the unmodified edges form infinite paths along the a and b directions, respectively, whereas in Fig. 2a, the unmodified edges form circuits, each of which can be regarded as an infinite path. The occurrence of an infinite path in the unmodified edges results from the presence of an unmodified edge between an adjacent pair of those vertices which are each attached to a modified edge. For the third procedure (Fig. 2d), modify edge *mr* between hexagons 1 and 2. Hexagon 2 must contain either 1 or 3 modified edges. Choice of the former requires that the line segments *lm*, *mn*, *no*, *op*, *pq*, *qr* and *rs* generate part of an infinite path. Line segment *qv* must be modified, and hexagon 3 cannot have three modified edges because *rs* has already been constrained. Hence the infinite path must continue around hexagon 3 through vertices t, u and v. Hexagon 4 is forced to match hexagon 2. Hexagons 5–9 are forced to contain three modified edges, and so on. Choice of three modified edges in hexagon 2 results merely in the interchange of the two types of hexagons.

Finally, there is an infinity of nets when three or four types of hexagons are allowed instead of the one or two types in the three simple nets. Radial, rather than lattice, symmetry occurs in some of these complex nets. Details will be given in another paper.

The properties of the simple nets of Fig. 2 are given in Table 1, and the nets are labeled with s for square-planar. Each $2D$ projection corresponds to two $3D$ nets. Net 278 s corresponds to square-planar edges around each inserted vertex. Adjacent $2D$ nets are translationally equivalent and superimposed in projection. For a fixed edge of length l, the dimensions of the hexagonal cell are $a = (2 + \sqrt{2})\, l$, $c = l\sqrt{2}$; these correspond to $a =$ 10.6 Å and $c = 4.5$ Å for $l = 3.2$ Å. Net 279 s is produced by the σ-transformation and has $a = 10.6$ Å and $c = l\,(1 + \sqrt{2}) = 7.7$ Å. Corresponding nets (278 and 279) with tetrahedral geometry around each inserted vertex have doubled c and smaller a because of the rotation of adjacent $2D$ nets (Fig. 3a). The space group symmetry is lowered from $P6/mmm$ for nets 278 s and 279 s to $P6/mcc$ for 278 and 279. The circuit symbols for the tetrahedral vertices consist of six numbers, but those for the square-planar vertices consist of only four. Because the cell repeats depend not only on the lengths of the edges of the framework but also on the angles between the edges, only approximate values for the tetrahedral nets are given in Table 2.

Nets 280 s and 281 s (Fig. 2d) are orthorhombic, as are nets 282 s and 283 s (Fig. 2b) and nets 284 s and 285 s (Fig. 2c). Also hexagons are distorted in projection if all edges of the nets are of equal length, as also are the hexagons 1–6 in Fig. 2a.

Table 1. Properties of 3-dimensional 4-connected nets with square-planar and tetrahedrally-connected vertices

Number	Building operation	Z_t	Circuit symbol	Z_e	Net	a(Å)	b(Å)	c(Å)
278s	$(6^3+2\wedge 6^2_{3,0})$	9	$(46^5)_2(4^26^2)_1$	9	*P6/mmm*	10.6	*a*	4.5
279s	$(6^3+2\wedge 6^2_{3,0})\cdot\sigma$	15	$(4^26^4)_4(6^4)_1$	15	*P6/mmm*	10.6	*a*	7.7
280s	$(6^3+2\wedge 6^2_{3,1})$	12	$(46^47)_2(4^26^2)_1$	12	*Pmam*	10.6	12	4.5
281s	$(6^3+2\wedge 6^2_{3,1})\cdot\sigma$	20	$(4^26^4)_4(6^4)_1$	20	*Pmam*	10.6	12	7.7
282s	$(6^3+2\wedge 6^2_2)$	3	$(46^48)_2(4^26^2)_1$	6	*Cmmm*	5.5	12	4.5
283s	$(6^3+2\wedge 6^2_2)\cdot\sigma$	5	$(4^26^4)_4(6^4)_1$	10	*Cmmm*	5.5	12	7.7
284s	$(6^3+2\wedge 6^2_{2'})$	6	$(46^48)_2(4^26^2)_1$	6	*Pbmm*	7	10	4.5
285s	$(6^3+2\wedge 6^2_{2'})\cdot\sigma$	10	$(4^26^4)_4(6^4)_1$	10	*Pbmm*	7	10	7.7
286s	$(3.12^2+2\wedge 12^2)$	9	$(346^4)_2(4^26^2)_1$	9	*P6/mmm*	13.5	*a*	4.5
287s	$(3.12^2+2\wedge 12^2)\cdot\sigma$	15	$(34^26^3)_2(6^4)_1$	15	*P6/mmm*	13.5	*a*	7.7
288s	$(4.8^2+2\wedge 4.8)$	12	$(46^48)_2(4^26^2)_1$	12	*P4/mmm*	12	*a*	4.5
289s	$(4.8^2+2\wedge 4.8)\cdot\sigma$	20	$(4^26^4)_4(6^4)_1$	20	*P4/mmm*	12	*a*	7.7
290s	$(4.8^2+2\wedge 8^2)$	6	$(4^26^4)_2(4^26^2)_1$	6	*P4/mmm*	8.5	*a*	4.5
291s	$(4.8^2+2\wedge 8^2)\cdot\sigma$	10	$(4^36^3)_4(6^4)_1$	10	*P4/mmm*	8.5	*a*	7.7
292s	$(4.8^2+2\wedge 4.8')$	6	$(46^48)_2(4^26^2)_1$	12	*Cmmm*	9	13	4.5
293s	$(4.8^2+2\wedge 4.8')\cdot\sigma$	10	$(4^26^4)_4(6^4)_1$	20	*Cmmm*	9	13	7.7
294s	$(4.8^2+2\wedge 4.8'')$	12	$(456^38)_2(4^26^2)_1$	12	*Pbmm*	9	12	4.5
295s	$(4.8^2+2\wedge 4.8'')\cdot\sigma$	20	$(4^256^3)_4(6^4)_1$	20	*Pbmm*	9	12	7.7
296s	$(4.6.12+2\wedge 4.6)$	18	$(46^48)_2(4^26^2)_1$	18	*P6/mmm*	16	*a*	4.5
297s	$(4.6.12+2\wedge 4.6)\cdot\sigma$	30	$(4^26^4)_4(6^4)_1$	30	*P6/mmm*	16	*a*	7.7
298s	$(4.6.12+2\wedge 4.12)$	18	$(46^5)_2(4^26^2)_1$	18	*Pb/mmm*	17	*a*	4.5
299s	$(4.6.12+2\wedge 4.12)\cdot\sigma$	30	$(4^26^4)_4(6^4)_1$	30	*P6/mmm*	17	*a*	7.7
300s	$(4.6.12+2\wedge 6.12)$	18	$(4^26^4)_2(4^26^2)_1$	18	*P6/mmm*	17	*a*	4.5
301s	$(4.6.12+2\wedge 6.12)\cdot\sigma$	30	$(4^36^3)_4(6^4)_1$	30	*P6/mmm*	17	*a*	7.7

Z_t = number of vertices in primitive unit cell; Z_c = number of vertices in conventional crystallographic unit cell. $(6^3+2\wedge 6^2_{3,0})$ indicates that a 2-connected vertex, 2, is inserted into the edge, 6^2, of a 6^3 net; there are 3 of these edges in two-thirds of the polygons, 6^2_3, and no edges in the other third of the polygons, 6^2_0, which combine to give $6^2_{3,0}$. When all polygons have the same insertion configuration, the subscripts are omitted. Primed subscripts for nets 284 and 285 indicate that vertices are inserted in a non-opposite non-incident edge configuration, as distinct from the unprimed subscripts of nets 282 and 283, whose vertices are inserted in opposite edges

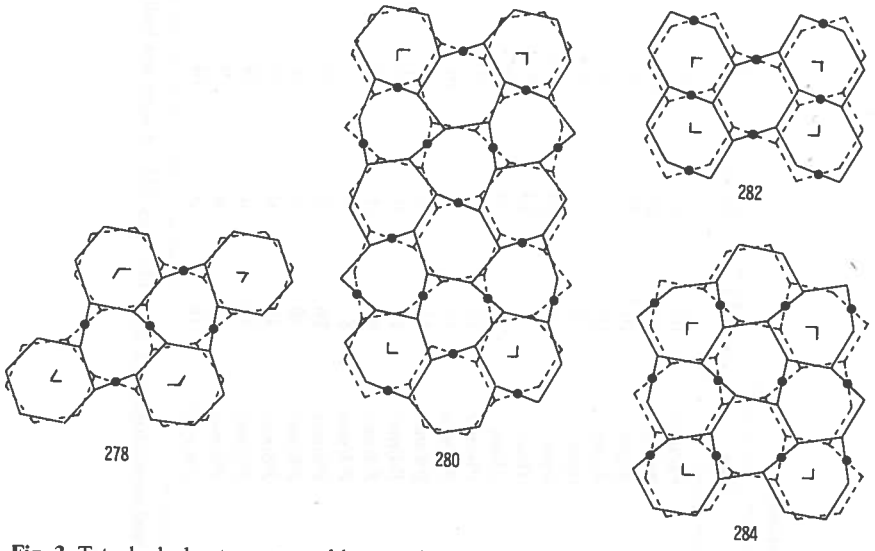

Fig. 3. Tetrahedral nets generated by rotation about the square-planar vertices in Fig. 2. Only the nets with the least geometrical distortion are shown

Derivation of the tetrahedral nets from the prototypes in Fig. 2 is not straightforward. Each tetrahedral vertex of type T_2 (Fig. 1e) can be generated in two orientations related by a clockwise and an anticlockwise rotation from the "neutral" square-planar geometry. Fig. 1e was deliberately drawn with an opposite rotation to that of Fig. 1c to illustrate the choice. There is an infinity of nets if there is no coupling between the rotations around adjacent square-planar vertices. Details will be given elsewhere, and Fig. 3 shows only the nets with the least geometrical distortion (Table 2). Thus in net 278, the regular hexagonal geometry is retained for each horizontal 6-ring. In net 282, the rotations are identical in each vertical row of the diagram, and are reversed between adjacent rows; this allows congruency of equivalent edges as each hexagon is sheared homogeneously. In nets 280 and 284, adjacent rotations are coupled to give the least geometrical distortion, but the edges are not congruent. For convenience of drawing, the split-edges were not elongated by $\sqrt{2}$ as was done in Fig. 2.

Net 278 is the tetrahedral framework of the beryl structure (Table 3; Fig. 4a) in which each 6-ring of silicate tetrahedra represents unmodified vertices of the 6^3 nets (Fig. 3) and each BeO_4 tetrahedron corresponds to an initial 2-connected vertex modified by linkage and rotation. This net also corresponds to indialite (Table 3), in which all tetrahedra are occupied by both Si and Al. Ordering of the Al into specific tetrahedra of low

Table 2. Properties of 3-dimensional 4-connected nets with tetrahedrally connected vertices

Number	Building operation	Z_t^*	Circuit symbol	Z_0^*	Net	a(Å)	b(Å)	c(Å)
278	$(6^3+2\wedge 6^2_{3,0})$	18	$(46^5)_2(4^26^28^2)_1$	18	$P6/mcc$	10	a	9
279	$(6^3+2\wedge 6^2_{3,0})\cdot\sigma$	30	$(4^26^4)_4(6^49^2)_1$	30	$P6/mcc$	10	a	14
280	$(6^3+2\wedge 6^2_{3,1})$	24	$(46^47)_2(4^26^28^2)_1$	48	$Acam$	10	21	9
281	$(6^3+2\wedge 6^2_{3,1})\cdot\sigma$	40	$(4^26^4)_4(6^49^2)_1$	80	$Acam$	10	21	14
282	$(6^3+2\wedge 6^2_2)$	6	$(46^48)_2(4^26^28^2)_1$	12	$Imcb$	9	11	5.5
283	$(6^3+2\wedge 6^2_2)\cdot\sigma$	10	$(4^26^4)_4(6^48^2)_1$	20	$Icma$	11	14	5.5
284	$(6^3+2\wedge 6^2_{2'})$	12	$(46^48)_2(4^26^28^2)_1$	24	$Abam$	9	14	9
285	$(6^3+2\wedge 6^2_{2'})\cdot\sigma$	20	$(4^26^4)_4(6^48^2)_1$	40	$Abam$	9	14	15
286	$(3.12^2+2\wedge 12^2)$	18	$(346^4)_2(4^26^28^2)_1$	18	$P6/mcc$	13	a	9
287	$(3.12^2+2\wedge 12^2)\cdot\sigma$	30	$(34^26^3)_4(6^410^2)_1$	30	$P6/mcc$	13	a	14
288	$(4.8^2+2\wedge 4.8)$	24	$(46^48)_2(4^26^4)_1$	24	$P4/mcc$	11	a	9
289	$(4.8^2+2\wedge 4.8)\cdot\sigma$	40	$(4^26^4)_4(6^6)_1$	40	$P4/mcc$	11	a	14
290	$(4.8^2+2\wedge 8^2)$	12	$(4^26^4)_2(4^26^28^2)_1$	12	$P4/mcc$	8	a	9
291	$(4.8^2+2\wedge 8^2)\cdot\sigma$	20	$(4^36^3)_4(6^410^2)_1$	20	$P4/mcc$	8	a	14
296	$(4.6.12+2\wedge 4.6)$	36	$(46^48)_2(4^26^4)_1$	36	$P6/mcc$	16	a	9
297	$(4.6.12+2\wedge 4.6)\cdot\sigma$	60	$(4^26^4)_4(6^6)_1$	60	$P6/mcc$	16	a	14
298	$(4.6.12+2\wedge 4.12)$	36	$(46^5)_2(4^26^4)_1$	36	$P6/mcc$	16	a	9
299	$(4.6.12+2\wedge 4.12)\cdot\sigma$	60	$(4^26^4)_4(6^6)_1$	60	$P6/mcc$	16	a	14
300	$(4.6.12+2\wedge 6.12)$	36	$(4^26^4)_2(4^26^28^2)_1$	36	$P6/mcc$	16	a	9
301	$(4.6.12+2\wedge 6.12)\cdot\sigma$	60	$(4^36^3)_4(6^49^2)_1$	60	$P6/mcc$	16	a	14

Z_t = number of vertices in primitive unit cell; Z_c = number of vertices in conventional crystallographic unit cell. Nets 292–5 were not built, but can be envisaged from the data for nets 292s–5s in Table 1

Table 3. Minerals based on the nets of Table 2

Mineral	Formula	a(Å)	b(Å)	c(Å)	Space group	Net	Ref.
Beryl	$Al_2[Be_3Si_6O_{18}]$	9.2088(5)	a	9.1896(7)	$P6/mcc$	278	[1][a]
Indialite	$(Mg,Fe)_2[Al_4Si_5O_{18}]$	9.800(3)	a	9.345(3)	$P6/mcc$	278	[2][a]
Cordierite	$(Mg,Fe)_2[Al_4Si_5O_{18}]$	17.079(3)	9.730(2)	9.356(2)	$Cccm$	278	[3][a]
Sekaninaite	$(Fe,Mg)_2[Al_4Si_5O_{18}]$	17.186	9.827	9.298	$Cccm$	278	[4]
Armenite	$BaCa_2[Al_6Si_9O_{30}] \cdot 2H_2O$	10.69	a	13.90	$P6/mcc$	279	[5][a]
Brannockite	$KSn_2[Li_3Si_{12}O_{30}]$	10.0167(2)	a	14.2452	$P6/mcc$	279	[6]
Darapiosite	$KNa_2Zr[Li(Mn,Zn)_2Si_{12}O_{30}]$	10.32	a	14.39	$P6/mcc$	279	[7]
Eifelite	$KNa_3Mg[Mg_3Si_{12}O_{30}]$	10.137(5)	a	14.223(6)	$P6/mcc$	279	[8]
Merrihueite	$(K,Na)(Fe,Mg)_2[(Fe,Mg)_3Si_{12}O_{30}]$	10.16(6)	a	14.32(6)	$P6/mcc$	279	[9]
Synthetic	$K_2Mg_2[Mg_3Si_{12}O_{30}]$	10.222(2)	a	14.152(2)	$P6/mcc$	279	[10][a]
Milarite	$KCa_2[AlBe_2Si_{12}O_{30}] \cdot H_2O$	10.420(2)	a	13.810(9)	$P6/mcc$	279	[11][a]
Osumilite	$(K,Na)(Fe^{2+},Mg)_2[Al,Fe^{3+})_3(Si,Al)_{12}O_{30}] \cdot H_2O$	10.155(1)	a	14.284(4)	$P6/mcc$	279	[12][a]
Osumilite-(Mg)	$(K,Na)(Mg,Fe^{2+})[(Al,Fe^{3+})_3(Si,Al)_{12}O_{30}] \cdot H_2O$	10.126(2)	a	14.319(3)	$P6/mcc$	279	[13][a]
Roedderite	$(Na,K)_2(Mg,Fe^{2+})_2[(Mg,Fe^{2+})_3Si_{12}O_{30}]$	10.142(5)	a	14.281(6)	$P6/mcc$	279	[8]
Sogdianite	$(K,Na)_2(Zr,Fe,Ti)[Li_2(Li,Al)Si_{12}O_{30}]$	10.083(5)	a	14.24(1)	$P6/mcc$	279	[5][a]
Sugilite	$(K,Na)(Na,Fe^{3+})_2[Li_2(Al,Fe^{3+})Si_{12}O_{30}]$	10.007(2)	a	14.000(2)	$P6/mcc$	279	[14][a]
Yagiite	$(Na,K)Mg_2[(Al,Mg)_3(Si,Al)_{12}O_{30}]$	10.09(1)	a	14.20(3)	$P6/mcc$	279	[15]
Steacyite	$(K,\square)Th[(Na,Ca)_2Si_8O_{20}]$	7.58(1)	a	14.77(2)	$P4/mcc$	291	[16][a], [17]

References: [1] Morosin (1972); [2] Meagher and Gibbs (1977); [3] Cohen et al. (1977); [4] Stanek and Miskovsky (1975); [5] Bakakin et al. (1975); [6] White et al. (1973); [7] Semenov et al. (1975); [8] Abraham et al. (1983); [9] Dodd et al. (1965); [10] Khan et al. (1972); [11] Černý et al. (1980); [12] Brown and Gibbs (1968); [13] Hesse and Seifert (1982); [14] Kato et al. (1976); [15] Bunch and Fuchs (1969); [16] Richard and Perrault (1972); [17] Perrault and Szymański (1982)

[a] Structure refinement

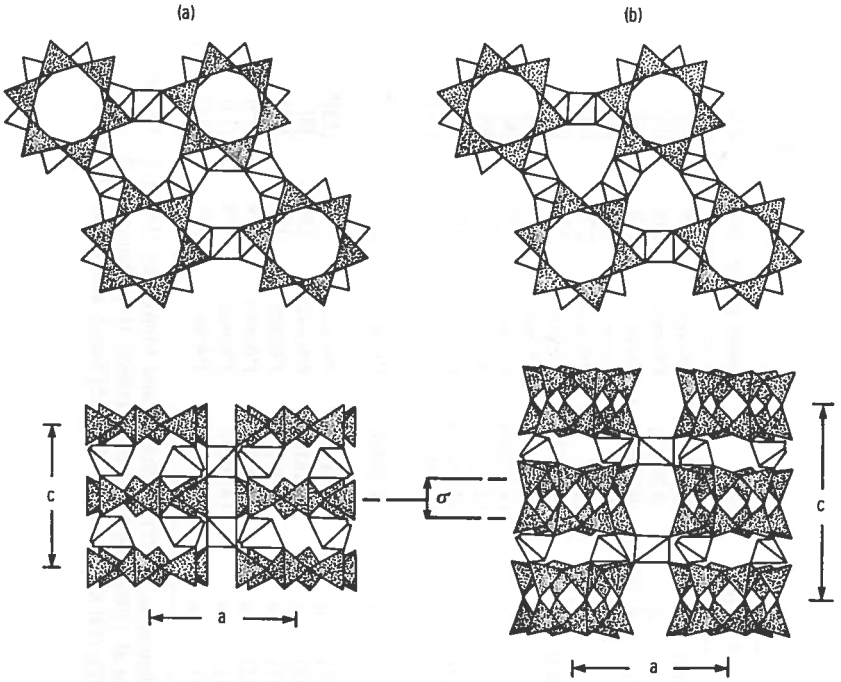

Fig. 4. Plans and elevations of the crystal structures of (a) beryl and (b) milarite. The operation of the σ-transformation is shown; the Si_6O_{18} ring in beryl has horizontal mirror symmetry, and the σ-transformation generates two such hexagonal rings, one either side of the horizontal mirror, that fuse at the mirror plane to form an $Si_{12}O_{30}$ double-ring

cordierite (Table 3) lowers the symmetry from hexagonal to orthorhombic. The ordering patterns in beryl and cordierite are just two out of the infinite number of possible arrangements for ordering of the tetrahedral species. The corresponding coloring of the vertices is explored elsewhere.

Net 279 is represented by the structure of milarite (Fig. 4b) and 12 other minerals listed in Table 3. The horizontal σ-transformation converts each 6-ring of the beryl structure into a double 6-ring. Both the beryl and milarite structure types contain cavities within the tetrahedral framework which can contain molecules including H_2O, Ar and CO_2, and cations (e.g. K and Ca in milarite). There is considerable flexibility in the geometrical and chemical properties, but the extent of the ranges (e.g. for substitution of Li for Be in Cs-rich beryl; Hawthorne and Černý, 1977) has not been explored.

No structures were found which matched nets 278–285 s (Table 1). Synthesis should be tried for appropriate chemical compositions involving mixed species known to adopt tetrahedral and square-planar coordination.

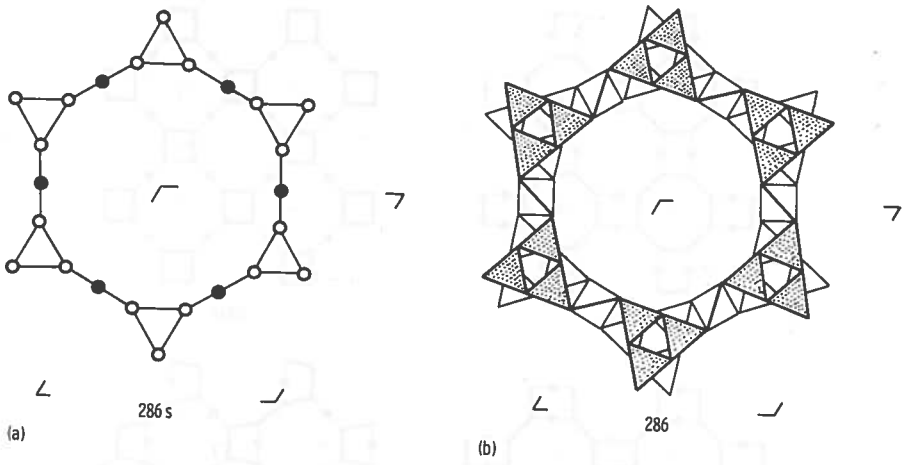

Fig. 5. Nets generated from the 3.12^2 $2D$ net. (a) Plan of nets 286 s and 287 s in which each 12^2 edge is converted into a square-planar vertex. (b) Plan of a polyhedral representation of a TO_4 framework based on nets 286 and 287. Each line connects a pair of adjacent O positions

Enumeration for the 3.12^2 net

From the possible nets, only the ones analogous to those of beryl and milarite are displayed in Fig. 5. Insertion of a vertex in every edge of type 12^2 gives rise to nets 286 s and 287 s (Table 1; Fig. 5a) and nets 286 and 287 (Table 2; Fig. 5b). The first diagram is a plan of the edges connecting the tetrahedral and square-planar vertices. The second diagram shows the outlines of tetrahedra in a TO_4 framework, in which tetrahedra viewed down a diad rotation axis link the tetrahedra of the rotated 3-rings. All these nets have large channels bounded by non-planar 18-rings with a free diameter comparable to that for a planar 14-ring.

Enumeration for the 4.8^2 net

Fig. 6 shows the four simple ways in which two-connected vertices may be introduced into edges of the 4.8^2 net. Conversion of each two-connected vertex into a square-planar vertex connecting parallel $2D$ nets produces $3D$ nets 288 s, 290 s, 292 s and 294 s (Table 1). A horizontal sigma transformation produces the $3D$ nets 289 s, 291 s, 293 s and 295 s (Table 1). The first two nets of each quartet retain the tetragonal symmetry from the 4.8^2 net, but the other nets are orthorhombic. Conversion of each square-planar vertex into a tetrahedral vertex produces an infinity of $3D$ nets, and only

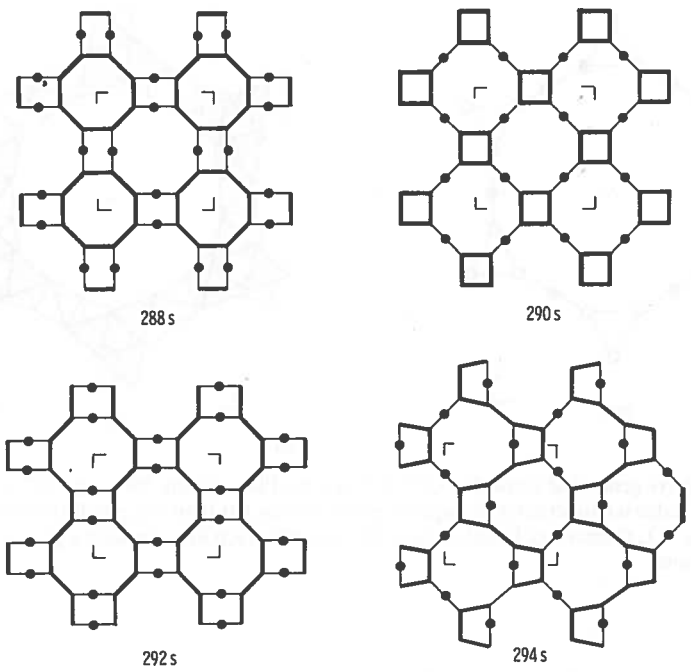

Fig. 6. Four simple ways of inserting 2-connected vertices into alternate edges of the 4.8^2 net

those with tetragonal symmetry are listed in Table 2. Net 290 and its σ-product net 291, are obtained from nets 290 s and 291 s by rotation of 4-rings in a clockwise direction in odd-numbered layers and an anticlockwise direction in even-numbered layers. Fig. 7 shows a plan in which a TO_4 framework is represented by the O–O edges. Net 288 and its σ-product net 289 are similarly obtained from nets 288 s and 289 s by rotation of 8-rings, and the drawing in Fig. 7 shows the T–T edges.

The nets 288–291 are closely analogous to those of the beryl and milarite type obtained from the 6^3 net. They have the same c dimension and stoichiometry ($T'_2T_4O_{12}$, 288 and 290; $T'_2T_8O_{20}$, 289 and 291). For net 291, 8-coordinated tetragonal antiprismatic sites alternate with 12-coordinated sites down the centers of the channels in a framework of type TO_4. The corresponding stoichiometry, $^{[12]}A^{[8]}B[T'_2T_8O_{20}]$, together with the space group, $P4/mcc$, and cell dimensions (Table 2) match with those (Table 3) of steacyite, $KTh[(Na,Ca)Si_8O_{20}]$. In detail, the (Na,Ca) in the T′ position has four short bonds to the tetrahedrally-arranged oxygens and four longer bonds to the adjacent four bridging oxygens of the Si_8O_{20} groups. Thorium and K occupy the A and B sites respectively, and vacancies seem to play an important role in the structure.

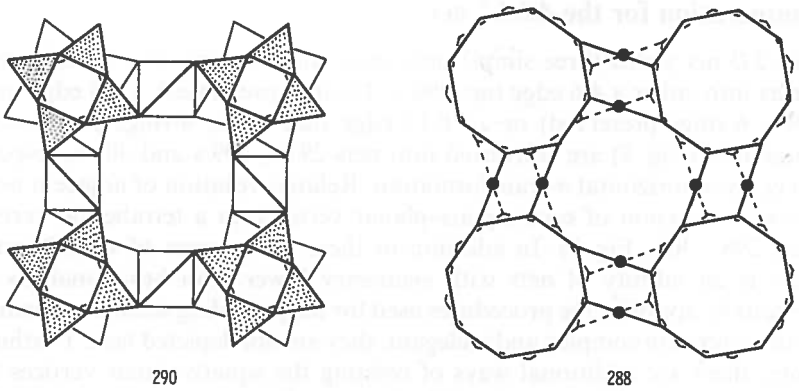

Fig. 7. Two simple tetrahedral nets obtained from the 4.8^2 net. For net 290, the lines show Q—O edges for a TO_4 framework. For net 288, the T—T linkages are shown. Each dot is a converted square-planar vertex. Both diagrams show projections down the tetragonal axis

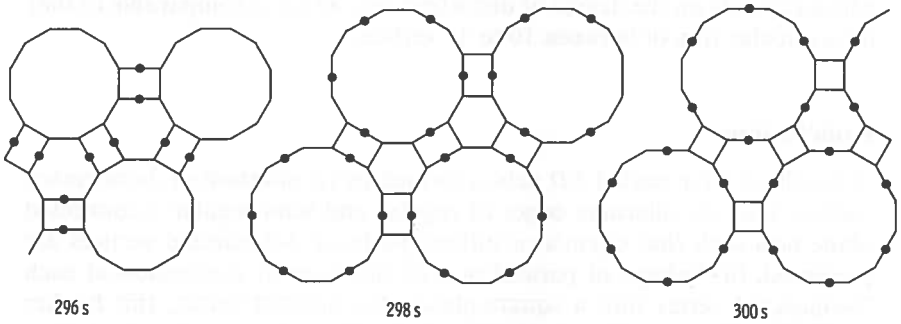

Fig. 8. Three simple ways of inserting 2-connected vertices into alternate edges of the 4.6.12 net

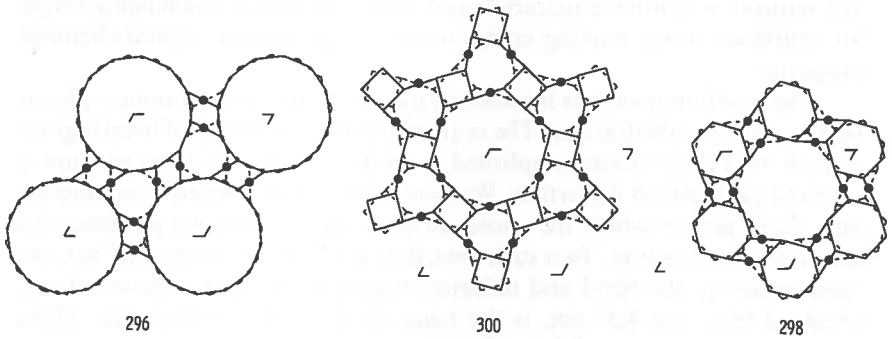

Fig. 9. Three simple tetrahedral nets obtained from the 4.6.12 net. Each line joints two vertices. Each dot is a tetrahedral vertex converted from a square-planar vertex

Enumeration for the 4.6.12 net

This $2D$ net yields three simple nets upon introduction of a 2-connected vertex into either a 4.6 edge (net 296 s; 12-rings preserved), a 4.8 edge (net 298 s; 6-rings preserved) or an 8.12 edge (net 300 s; 4-rings preserved). These nets (Fig. 8) are converted into nets 297 s, 299 s and 301 s, respectively, by a horizontal σ-transformation. Relative rotation of adjacent nets allows conversion of each square-planar vertex into a tetrahedral vertex (nets 298 – 301; Fig. 9). In addition to these two groups of six $3D$ nets, there is an infinity of nets with symmetry lower than hexagonal, as is obvious by applying the procedures used for the preceding sections. Because all these nets are complex and inelegant, they are not depicted here. Furthermore, there are additional ways of twisting the square-planar vertices to obtain tetrahedral linkages in a TO_4 framework.

All six of the new tetrahedral nets (296 – 301) have large cylindrical channels. Those of 296 and 297 are bounded by circular planar 12-rings, while those of 298 – 301 are circumscribed by non-planar 18-rings. The non-planarity reduces the effective free diameter of these 18-rings to a value which depends on the degree of distortion, but which is comparable to that for a circular ring of between 10 to 12 vertices.

Conclusions

A family of 4-connected $3D$ nets is formed by (i) insertion of 2-connected vertices into the alternate edges of regular and semi-regular 3-connected plane nets such that circuits or infinite paths of 3-connected vertices are preserved, (ii) linkage of parallel nets of this type by conversion of each 2-connected vertex into a square-planar 4-connected vertex, (iii) further evolution of each such new 4-connected $3D$ net by a σ-transformation through the plane of each original 3-connected $2D$ net. This family of nets with both tetrahedral and square-planar vertices is not yet represented by any natural or synthetic material, and would provide a challenging target for syntheses using starting components of appropriate crystal-chemical properties.

A second family of nets is obtained by conversion of each square-planar vertex into a tetrahedral one. The required relative rotations of local regions of each $3D$ net can be accomplished in an infinity of ways if no account is taken of geometrical distortion. We have deliberately chosen to enumerate only those nets in which the choice of the relative rotations produces the least overall distortion. Two such nets, derived from the original 6^3 net, are represented by the beryl and milarite structures. A third tetrahedral net, obtained from the 4.8^2 net, is the basis of the steacyite structure. Three tetrahedral nets obtained from the 4.6.12 net contain cylindrical channels bounded by either a circular 12-ring or a non-planar 18-ring.

Acknowledgements. We thank Mobil Corporation for a grant-in-aid to the Department of Geophysical Sciences which covered the expenses of FCH. Thanks are also due to NSF-CHE for grant 84-05167, and N. Weber for technical assistance.

References

Abraham, K., Gebert, W., Mendenbach, O., Schreyer, W., Hentschel, G.: Eifelite, $KNa_3Mg_4Si_{12}O_{30}$, a new mineral of the osumilite group with octahedral sodium. Contrib. Mineral. Petrol. **82**, 252–258 (1983)

Bakakin, V. V., Balko, V. P., Solov'eva, L. P.: Crystal structures of milarite, armenite and sogdianite. Sov. Phys. Crystallogr. **19**, 460–462 (1975)

Bennett, J. M., Smith, J. V.: Enumeration of 4-connected 3-dimensional nets and classification of framework silicates. 3 *D* nets based on the 4.6.12 and $(4.6.10)_4(6.6.10)_1$ 2 *D* nets. Z. Kristallogr. **171**, 65–68 (1985)

Brown, G. E., Gibbs, G. V.: Refinement of the crystal structure of osumilite. Am. Mineral. **54**, 101–116 (1969)

Bunch, T. E., Fuchs, L. H.: Yagiite, a new sodium-magnesium analogue of osumilite. Am. Mineral. **54**, 14–18 (1969)

Černý, P., Hawthorne, F. C., Jarosewich, E.: Crystal chemistry of milarite. Can. Mineral. **18**, 41–57 (1980)

Cohen, J. P., Ross, F. K., Gibbs, G. V.: An X-ray and neutron diffraction study of hydrous low cordierite. Am. Mineral. **62**, 67–78 (1977)

Dodd, R. T., van Schmus, W. R., Marvin, U. B.: Merrihueite, a new alkaliferromagnesium silicate from the Mezö-Maddras chondrite. Science **149**, 972–974 (1965)

Hawthorne, F. C., Černý, P.: The alkali-metal positions in Cs-Li beryl. Can. Mineral. **15**, 414–421 (1977)

Hesse, K. F., Siefert, F.: Site-occupancy refinement of osumilite. Z. Kristallogr. **160**, 179–186 (1982)

Kato, T., Miura, Y., Murakami, N.: Crystal structure of sugilite. Mineral. J. (Tokyo) **8**, 184–192 (1976)

Khan, A. A., Baur, W. H., Forbes, W. C.: Synthetic magnesian merrihueite, dipotassium pentamagnesium dodecasilicate: a tetrahedral magnesiosilicate framework crystal structure. Acta Crystallogr. **B28**, 267–272 (1972)

Meagher, E. P., Gibbs, G. V.: The polymorphism of cordierite: II. The crystal structure of indialite. Can. Mineral. **15**, 43–49 (1977)

Morosin, B.: Structure and thermal expansion of beryl. Acta Crystallogr. **B28**, 1899–1903 (1972)

Perrault, G., Szymanski, J. T.: Steacyite, a new name and a re-evaluation of the nomenclature of "ekanite"-group minerals. Can. Mineral. **20**, 59–64 (1982)

Richard, P., Perrault, G.: La structure cristalline de l'ekanite $Th_{2-x}(Na, Ca)_{4-y}K_{2-z}Si_{16}O_{40}$. Acta Crystallogr. **B28**, 1994–1999 (1972)

Semenov, E. I., Dusmatov, V. D., Khomyakov, A. P., Voronkov, A. A., Kazakova, M. E.: Darapiosite, a new mineral of the milarite group. Zap. Vses. Mineral. O. **104**, 583–584 (1975)

Shoemaker, D. P., Robson, H. E., Broussard, L.: The "sigma transformation" interrelating certain known and hypothetical zeolite structures. "*Molecular Sieves*", (Ed. J. B. Uytterhoeven), pp. 138–143. Leuven University Press, Leuven (1973)

Smith, J. V.: Enumeration of 4-connected 3-dimensional nets and classification of framework silicates. I. Perpendicular linkages from simple hexagonal net. Am. Mineral. **62**, 703–709 (1977)

Smith, J. V.: Enumeration of 4-connected 3-dimensional nets and classification of framework silicates. II. Perpendicular and near-perpendicular linkages from 4.8^2, 3.12^2 and 4.6.12 nets. Am. Mineral. **63**, 960–969 (1978)

Smith, J. V.: Enumeration of 4-connected 3-dimensional nets and classification of framework silicates. III. Combination of helix, and zigzag, crankshaft and saw chains with simple 2*D* nets. Am. Mineral. **64**, 551–562 (1979)
Smith, J. V.: Enumeration of 4-connected 3-dimensional nets and classification of framework silicates: combination of 4-1 chain and 2*D* nets. Z. Kristallogr. **165**, 191–198 (1983)
Smith, J. V., Bennett, J. M.: Enumeration of 4-connected 3-dimensional nets and classification of framework silicates: the infinite set of ABC-6 nets; the Archimedean and σ-related nets. Am. Mineral. **66**, 777–788 (1981)
Smith, J. V., Bennett, J. M.: Enumeration of 4-connected 3-dimensional nets and classification of framework silicates: linkages from the two $(5^2.8)_2(5.8^2)_1$ 2*D* nets. Am. Mineral. **69**, 104–111 (1984)
Smith, J. V., Dytrych, W. J.: Nets with channels of unlimited diameter. Nature **309**, 607–608 (1984)
Stanek, J., Miskovsky, J.: Sekaninaite, a new mineral of the cordierite series, from Dolni Bory, Czechoslovakia. Scr. Fac. Sci. Nat. Ujep. Brun., geol. **1**, 21–30 (1975)
White, J. S. Jr., Arem, J. E., Nelen, J. A., Leavens, P. B., Thomssen, R. W.: Brannockite, a new tin mineral. Mineral. Rec. **4**, 73–76 (1973)